DIVISION OF MOLECULAR NEUROBIOLOGY

Professor
NODA, Masaharu

Associate Professor
SHINTANI, Takafumi

Assistant Professors:	SAKUTA, Hiraki
	HIYAMA, Takeshi
Technical Staff:	TAKEUCHI, Yasushi
NIBB Research Fellows:	YOSHIDA, Masahide
	KUBOYAMA, Kazuya
Postdoctoral Fellows:	FUJIKAWA, Akihiro
	SUZUKI, Ryoko
	NISHIHARA, Eri
	MATSUMOTO, Masahito
Graduate Students:	TANI, Sachiko
	SAKURABA, Jyuichi
	MIYAZAKI, Yuriko
Technical Assistants:	HATTORI, Nobuko
	TOMITA, Nao
	MIURA, Seiko
	NAKANISHI, Norie
	DOKYO, Yumi
	MIYAZAKI, Emi
	WADA, Kotoe
Secretary:	KODAMA, Akiko

We have been studying the molecular and cellular mechanisms underlying the development of the vertebrate central nervous system (CNS), mainly using the visual systems of chicks and mice. This research covers many developmental events including the patterning of the retina, neuronal terminal differentiation, axonal navigation, branching and targeting, synapse formation, refinement and plasticity. The scope of our interests also encompasses the mechanisms for various functions of the mature brain, including body-fluid regulation, behavior control, learning, and memory.

I. Mechanisms for neural circuit formation

Topographic maps are a fundamental feature of neural networks in the nervous system. We have long studied the molecular mechanisms for regional specification in the developing retina as the basis of the topographic retinotectal projection. We are now focusing our attention on the molecular mechanisms underlying axon branching and arborization for synapse formation, along with elimination of mistargeted axons and branches. Among the region-specific molecules in the developing retina, we have already found several molecules that induce abnormal branching or arborization when their expression was experimentally manipulated *in vivo*. One is adenomatous polyposis coli 2 (APC2), which is preferentially expressed in the nervous system from early developmental stages through to adulthood.

APC2 is distributed along microtubules in growth cones as well as axon shafts of retinal axons. The knockdown of *Apc2* in chick retinas reduced the stability of microtubules in retinal axons and yielded abnormal behaviors including a reduced response to ephrin-A2 and misprojection in the

tectum without making clear target zones. Recently, we generated *Apc2*-deficient mice by a gene-targeting technique. We have found that the mutant mouse displays severe laminary defects in some brain regions including the cerebral cortex and cerebellum. We are now analyzing the phenotype of the *Apc2*-deficient mouse in more detail to clarify the function of APC2 in the development of the CNS.

II. Development of direction-selective retinal ganglion cell subtypes

Visual information is transmitted to the brain by roughly a dozen distinct types of retinal ganglion cells (RGCs) defined by characteristic morphology, physiology, and central projections. However, because few molecular markers corresponding to individual RGC types are available, our understanding of how these parallel pathways develop is still in its infancy.

The direction of image motion is coded by direction-selective (DS) ganglion cells in the retina. Particularly, the ON DS ganglion cells are critical for mediating the optokinetic reflex. We generated a knock-in mouse in which *SPIG1*-expressing cells are labeled with GFP. We successfully visualized both upward- motion-preferring and downward-motion-preferring ON DS ganglion cells (SPIG1$^+$ and SPIG1$^-$ ganglion cells, respectively) by a combination of genetic labeling and conventional retrograde labeling in the medial terminal nucleus.

A key circuit module of DS ganglion cells is a spatially asymmetric inhibitory input from starburst amacrine cells in the retina. However, it was not known how and when this circuit asymmetry is established during development. Therefore, we photostimulated mouse starburst cells targeted with channelrhodopsin-2 (CR-2) while recording from single SPIG1$^+$ DS cells. We then followed the spatial distribution of synaptic strengths between starburst and DS cells during early postnatal development before these neurons can respond to physiological light stimuli, along with confirmation of connectivity by monosynaptically restricted trans-synaptic rabies viral tracing. As a result, we found that random or symmetric synaptic connections from starburst amacrine cells are established as early as postnatal day 6, and that asymmetric inhibitory synaptic inputs are subsequently developed over a 2-day period (Figure 1).
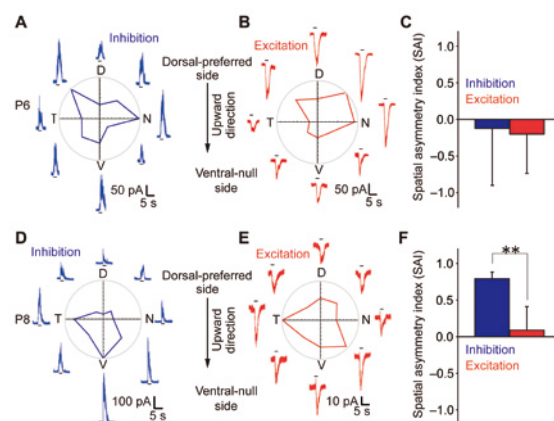

Figure 1. CR-2-assisted circuit mapping at P6 and P8. Recordings from SPIG1$^+$ cells at P6 (A–C) and P8 (D–F). (A–E) Inhibitory (A, D) and excitatory (B, E) postsynaptic currents elicited in a SPIG1$^+$ cell by the

photostimulation of the surrounding starburst amacrine cells. Polar plots are also shown. (C, F) Spatial asymmetry index (SAI) for inhibition and excitation. Error bars, s.d.

Analysis of gene-expression profiles in the two types of ON DC ganglion cells is now under way. This will shed light on molecular mechanisms underlying the differentiation and distinct circuit formation of the two DS ganglion cell types.

III. Physiological roles of protein tyrosine phosphatase receptor type Z

Protein-tyrosine phosphatase receptor type Z (Ptprz, also known as PTPζ/RPTPβ) is a member of the R5 receptor-like protein tyrosine phosphatase (RPTP) subfamily. Ptprz is predominantly expressed in the brain and its physiological importance has been demonstrated through studies with *Ptprz*-deficient mice. Ptprz modulates hippocampal synaptic plasticity: adult *Ptprz*-deficient mice display impairments in spatial and contextual learning. Ptprz is expressed also in the stomach, where it is used as a receptor for VacA, a cytotoxin secreted by *Helicobacter pylori*: *Ptprz*-deficient mice are resistant to gastric ulcer induction by VacA. Although our understanding of the physiological functions of Ptprz is thus advancing, our knowledge about its biochemical properties such as substrate specificity are still limited.

We previously identified G protein-coupled receptor kinase interactor 1 (Git1), membrane-associated guanylate kinase, WW and PDZ domain-containing 1 (Magi1), and GTPase-activating protein for Rho GTPase (p190RhoGAP) as substrates for Ptprz by developing a new genetic method named "yeast substrate-trapping system". We had already identified a dephosphorylation site at Tyr-1105 of p190RhoGAP; however, the structural determinants employed for substrate recognition of Ptprz have not been fully defined.

This year, we revealed that Ptprz selectively dephosphorylates Git1 at Tyr-554, and Magi1 at Tyr-373 and Tyr-858 by *in vitro* and cell-based assays. Of note, alignment of the primary sequences surrounding the target phosphotyrosine residue in these three substrates showed considerable similarity, suggesting a consensus motif for recognition by Ptprz (Figure 2A). We then estimated the contribution of surrounding individual amino acid side chains to the catalytic efficiency by using fluorescent peptides based on the Git1 Tyr-554 sequence *in vitro* (Figure 2B), and thereby deduced the typical substrate motif for the catalytic domain of Ptprz (Figure 2C). Furthermore, we found by database screening that the substrate motif is present in several proteins, including paxillin at Tyr-118, its major phosphorylation site (Figure 2A). Expectedly, we verified that Ptprz efficiently dephosphorylates paxillin at this site in cells.

Although initially viewed as broad specificity "housekeeping" enzymes, PTPs are actually highly selective enzymes. Our knowledge of substrates for Ptprz suggests that Ptprz dephosphorylates multiple proteins associated with actin remodeling, which plays important roles in synaptic plasticity in the adult brain and cell adhesion/migration of epithelial cells.
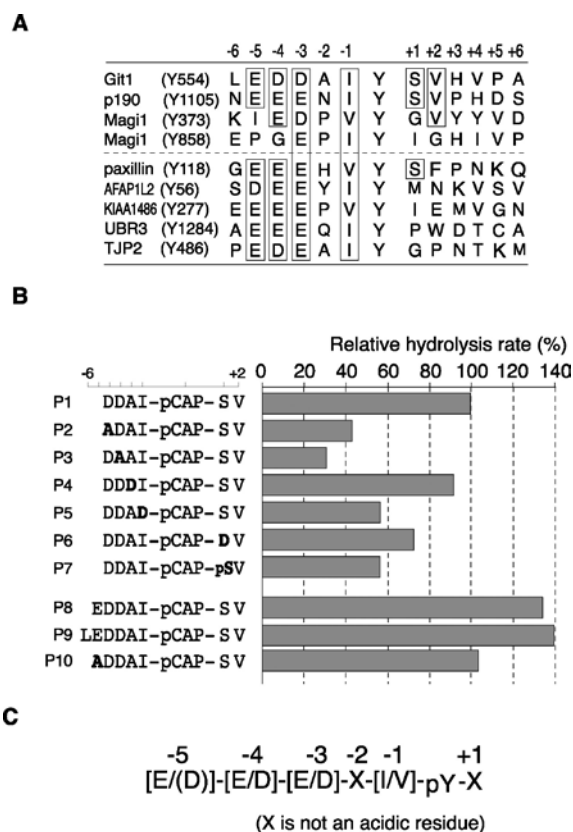

Figure 2. Identification of the substrate motif for Ptprz. (A) Primary sequences surrounding the target phosphotyrosine residues located in Git1 (Tyr-554), p190RhoGAP (Tyr-1105), Magi1 (Tyr-373 and Tyr-858), and paxillin (Tyr-118) aligned, together with four substrate candidates, AFAP1L2 (Tyr-56), KIAA1486 (Tyr-277), UBR3 (Tyr-1284), and TJP2/ZO-2 (Tyr-486). Boxed residues are conserved in at least three substrate sequences. (B) Kinetic analysis for the hydrolysis of Git1-derived peptide substrates by PtprzICR *in vitro*. The amino acid sequences of the substrate peptides (P1–10) used in this study are shown on the left of the figure. P1, P8, and P9 peptides correspond to Git1550–556, Git1549–556, and Git1548–556, respectively, except that the Tyr residue at 554 is replaced with a phosphotyrosine mimic, pCAP. P1–P7 and P10 peptides are Git1 peptide derivatives, in which the substituted amino acid residues are shown in bold. (C) Proposed consensus substrate-site motif for the PTP catalytic domain of Ptprz.

IV. Brain systems for body-fluid homeostasis

Mammals have a set of homeostatic mechanisms that work together to maintain body-fluid osmolality at near 300 mOsm/kg through the intake or excretion of water and salt. Although this homeostatic osmoregulation is vital, the mechanisms for the detection of these fluctuations have not been fully elucidated. To date, transient receptor potential vanilloid 1 (TRPV1), a cation channel, has been implicated in body-fluid homeostasis *in vivo* based on studies with the *TRPV1*-knockout mouse. However, the response of TRPV1 to hypertonic stimuli has not been demonstrated with heterologous expression systems so far, despite intense efforts by several groups. Thus, the molecular entity of the hypertonic sensor *in vivo* still remains controversial.

Very recently, we found that the full-length form of TRPV1 is sensitive to an osmotic increase exclusively at around body temperature by using human embryonic kidney 293 cells

stably expressing rat TRPV1 (HEK293-TRPV1 cells). We applied a hypertonic solution (350 mOsm) to HEK293-TRPV1 cells at various temperatures from 24 to 40°C (Figure 3A and B, HEK293-TRPV1). When the extracellular environment was changed from an isotonic (300 mOsm) to hypertonic (350 mOsm) solution at 24°C, $[Ca^{2+}]_i$ increased only slightly in HEK293-TRPV1 cells, but not in native HEK293 cells (Figure 3A and B). Surprisingly, the magnitude of the osmosensitive response markedly increased with temperature, peaking at around 36°C, which is close to normal mammalian body temperature (~37°C) (Figure 3A and B). In contrast, control HEK293 cells did not respond to the hypertonic stimulus at any temperature. Importantly, the response at 36°C showed a robust increase over a hypertonic range, but a small decrease over a hypotonic range (Figure 3C). A TRPV1 antagonist, capsazepine, and a nonspecific TRP channel inhibitor, ruthenium red, completely blocked the increase in $[Ca^{2+}]_i$. These results endorse the view that the full-length form of TRPV1 is able to function as a sensor of hypertonic stimuli.

We also demonstrated that the osmosensitivity of TRPV1 at 36°C is further enhanced by other activating stimuli, such as protons (pH) or capsaicin, indicating that osmosensitivity of TRPV 1 is synergistically enhanced by these distinct activating stimuli. (Figure 3D and E). Our findings thus indicate that TRPV1 integrates multiple different types of activating stimuli, and that TRPV1 is sensitive to hypertonic stimuli under physiologically relevant conditions.
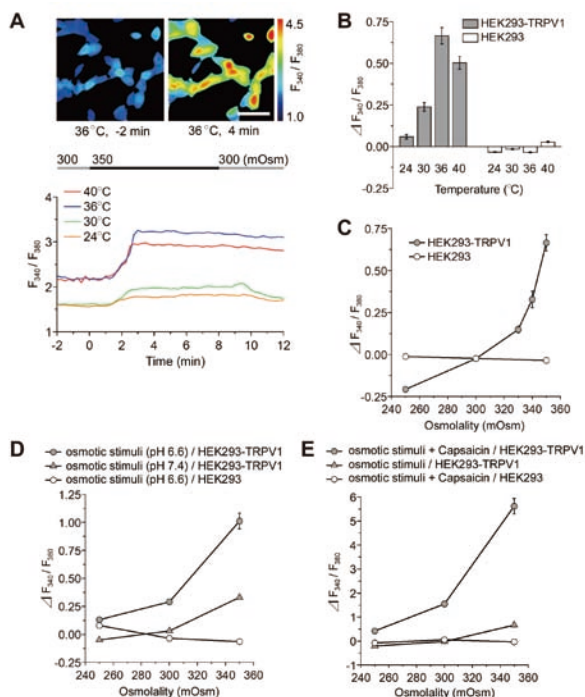
(gray) to 350 mOsm (black). (B) Summary of the change in the fluorescence ratio during perfusion with the hypertonic solution at various temperatures in HEK293-TRPV1 (filled bars) and HEK293 (open bars) cells. Data are differences between fluorescence ratios before and after the change of the solution. The maximal sensitivity of the HEK293-TRPV1 cells to the hypertonic stimulation was observed at 36°C. (C) Summary of the change in the fluorescence ratio during the perfusion of various solutions differing in osmolality at 36°C. Osmolality-dependent changes in the $[Ca^{2+}]_i$ were observed in HEK293-TRPV1 cells (filled circles), but not in HEK293 cells (open circles). (D) Summary of the change in the fluorescence ratio during the perfusion of solutions with the respective osmolality and pH at 36°C. The osmotic response of the $[Ca^{2+}]_i$ in HEK293-TRPV1 cells (filled circles) was enhanced by acidification over the entire osmolality range (compare with filled triangles). This was evident especially in the hypertonic range. (E) Summary of the change in the fluorescence ratio in HEK293-TRPV1 cells upon application of 1.5 nM capsaicin solutions with different osmotic strength. Response of TRPV1 to hyperosmolality was markedly potentiated in the presence of capsaicin (compare filled circles with filled triangles). No response was observed in HEK293 cells (open circles). Error bars, s.e.m.

Publication List

〔**Original papers**〕

● Fujikawa, A., Fukada, M., Makioka, Y., Suzuki, R., Chow, J.P., Matsumoto, M., and Noda, M. (2011). Consensus substrate sequence for protein-tyrosine phosphatase receptor type Z. J. Biol. Chem. *286*, 37137-37146.

● Nayak, G., Goodyear, R.J., Legan, P.K., Noda, M., and Richardson, G.P. (2011). Evidence for multiple, developmentally regulated isoforms of PTPRQ on hair cells of the inner ear. Dev. Neurobiol. *71*, 129-141.

● Nishihara, E., Hiyama, T.Y., and Noda, M. (2011). Osmosensitivity of transient receptor potential vanilloid 1 is synergistically enhanced by distinct activating stimuli such as temperature and protons. PLoS ONE *6*, e22246.

● Sakamoto, K., Bu, G., Chen, S., Takei, Y., Hibi, K., Kodera, Y., McCormick, L.M., Nakao, A., Noda, M., Muramatsu, T., and Kadomatsu, K. (2011). The premature ligand-receptor interaction during biosynthesis limits the production of growth factor midkine and its receptor LDL receptor-related protein 1 (LRP1). J. Biol. Chem. *286*, 8405-8413.

● Yonehara, K., Balint, K., Noda, M., Nagel, G., Bamberg, E., and Roska, B. (2011). Spatially asymmetric reorganization of inhibition establishes a motion-sensitive circuit. Nature *469*, 407-410.

Figure 3. Osmosensitivity of TRPV 1 is synergistically enhanced by distinct activating stimuli such as temperature and protons. (A) Temperature-dependent sensitivity to osmotic stimuli. Representative pseudo-color images of $[Ca^{2+}]_i$ in HEK293-TRPV1 cells at 2 min before (upper left) and 4 min after (upper right) perfusion with a hypertonic solution (350 mOsm) at 36°C. Representative single cell traces of the fluorescence ratio at a temperature of 24, 30, 36, or 40°C (lower graph). The line on the top indicates the timing of the change from 300 mOsm